Long-term persistency of a strong non-dipole field in the South Atlantic

Wellington P de Oliveira, Gelvam A Hartmann, Filipe Terra-Nova, Natália G Pasqualon, Jairo F Savian, Evandro F Lima, Fernando R da Luz, Ricardo I F Trindade

nature communications

Article

https://doi.org/10.1038/s41467-024-53688-2

Long-term persistency of a strong non-dipole field in the South Atlantic

Received: 20 March 2024

Accepted: 18 October 2024

Published online: 01 November 2024

Check for updates

Wellington P. de Oliveira[1] ✉, Gelvam A. Hartmann[1], Filipe Terra-Nova[2], Natália G. Pasqualon[3,4], Jairo F. Savian[4], Evandro F. Lima[4], Fernando R. da Luz[4] & Ricardo I. F. Trindade[5]

Earth's magnetic field exhibits a dominant dipole morphology. Notwithstanding, significant deviations from the dipole are evident today, particularly the South Atlantic Anomaly (SAA), characterized by anomalously low-field intensity and high directional variability, diminishing the field's shielding effect. To assess the persistence of SAA-like features over multimillion-year scales, we combine paleomagnetic data from Trindade Island (20°30'S, 29°22'W) with an evaluation of paleosecular variation (PSV) over the past 10 Myr. We employ synthetic models to explore how the position and intensity of magnetic flux patches at the core-mantle boundary can influence the long-term field behavior. Here we present results that reveal anomalous field signatures in the South Atlantic and the Atlantic-Pacific hemispheric asymmetries are enduring features, likely linked to a bottom-up control of PSV by the inner core's heterogeneities but with contributions from mantle anomalies in the long-time range.

The Earth's magnetic field, generated by a self-sustaining dynamo, plays a crucial role in shielding the planet from solar charged particles, which can damage technological systems, disrupting satellite and communication operations and induce unwanted currents in power grids[1]. The main geomagnetic field is dominated by an axial dipole but outstanding non-dipolar features are observed, including regions of particularly weak field where the magnetic shielding is much less effective. Reconstructions of the temporal geomagnetic field evolution in the last decades to centuries have been obtained based on historical observations from observatory measurements and satellites, whereas archeomagnetic and paleomagnetic records cover the past from centuries to millions of years[2]. When averaged over a period, global geomagnetic field models[3–5] show that some of the non-dipole field structures persist over time.

The main non-dipole field feature at the Earth's surface is the so-called South Atlantic Anomaly (SAA), which has historically been characterized by the lowest total field intensity and pronounced directional variability[6]. Currently, the SAA encompasses a large area from Southern Africa to South America, strongly influencing the field observed in Brazil[7]. The recurrence of the SAA has been suggested during the past millennium based on archaeomagnetic data from Southern Africa[8,9] and Brazilian speleothem and sedimentary records[10–12]. SAA-type structures have also been episodically observed in paleomagnetic reconstruction models spanning the Holocene[13,14], 28–48 ka interval[15], the past 100 ka[16] and the 5.3–23 Ma[17] interval. Changes in the SAA location manifests at the core-mantle boundary (CMB) as the time-dependence of reversed flux patches (RFPs)[6,18]. Whether this feature and the corresponding hemispheric asymmetries have persisted over long periods is still a matter of debate[17]. Recent studies indicate a higher level of secular variation (SV) in the Southern Hemisphere relative to the Northern Hemisphere and in the Atlantic relative to the Pacific based on present, centennial[19] and multi-millennial[3,5] geomagnetic field models.

On million-year timescales, some results show signs of hemispherical field asymmetries over the past 10 Myr[4,20]. Paleomagnetic data from 8–10 Ma lava flows from Saint Helena Island[20,21] reveal

[1]Instituto de Geociências, Universidade Estadual de Campinas, Campinas, Brazil. [2]Nantes Université, Univ Angers, Le Mans Université, CNRS, Laboratoire de Planétologie et Géosciences, Nantes, France. [3]Department of Earth and Planetary Sciences, University of Hawai'i at Manoa, Honolulu, HI, USA. [4]Instituto de Geociências, Universidade Federal do Rio Grande do Sul, Porto Alegre, RS, Brazil. [5]Instituto de Astronomia, Geofísica e Ciências Atmosféricas, Universidade de São Paulo, São Paulo, SP, Brazil. ✉e-mail: oliveir@unicamp.br

anomalous behavior in the South Atlantic Ocean region, supported by low paleointensity and high dispersion of virtual geomagnetic poles (VGPs). Similarly, an average paleointensity estimate weaker than expected from a geocentric axial dipole (GAD) field was reported on the volcanic island of Tristan da Cunha for the 90–46 ka interval[22]. Some authors[8,20,22] hypothesized that the longevity of the anomalous field variability in that region could be related to a thermal heterogeneity at the CMB, influenced by the African large low shear velocity province (LLSVP), which may lead to the emergence of SAA-like features over millions of years[8]. Dynamo models that account for lower mantle heterogeneity recover the longitudes of persistent geomagnetic surface intensity minima and the southern tendency for a range of control parameters, though the relatively large latitude of the SAA seems more elusive[18].

The long-period variations of the geomagnetic field (~10^5–10^6 years) are referred to as paleosecular variation (PSV), which can be statistically evaluated in terms of the latitudinal pattern of VGP dispersion[23]. PSV studies[24,25] offer useful insights into the temporal evolution and morphology of the time-averaged field (TAF). Paleomagnetic data from igneous rocks, in particular lava flows, are commonly used to assess the PSV and TAF properties because they represent spot readings of the paleomagnetic field[2]. Analyses of the 0–10 Ma data sets[4,25] allow the investigation of longitudinal and latitudinal variations in the paleomagnetic field structure with a relatively low degree of influence of plate tectonic movement[2]. This information provides favorable conditions for examining long-term hemispheric field asymmetries. Investigations on this subject are relevant to better understand the geodynamo processes in the Earth's core. However, the global study of PSV and TAF is hampered by the paucity of paleomagnetic data, especially in the Southern Hemisphere, which represents only ~31% of the 0–10 Ma global database[25]. This highlights the need for new paleomagnetic records in this region to better constrain the long-term field behavior.

Here, we extend the paleomagnetic database in the Southern Hemisphere with high-quality paleodirection data from Pliocene-Pleistocene volcanic rocks collected at Trindade Island, the youngest Brazilian volcanic island in the South Atlantic Ocean. The Trindade island (Fig. 1) is well located to allow testing of the persistence of anomalous sources of the geomagnetic field in the South Atlantic region for the past few million years. Regional PSV and TAF models were then built using the 0–10 Ma data compilation[25] that provide evidence for the Pacific-Atlantic asymmetry of the paleomagnetic field. We also propose synthetic approaches to evaluate the relation of the intensity and position of reversed magnetic flux patches with the PSV latitudinal structure.

Results

Paleodirectional records from Trindade Island

The Trindade Island covers a small area of about 13.5 km^2 (elongated in the NW-SE direction) and is completely uninhabitable, situated in the eastern part of the Brazilian territory, on the South Atlantic Ocean (20°30′ S and 29°22′W) (Fig. 1). It was formed during the Tertiary as a result of the movement of the South American Plate over a mantle plume in its final stages of evolution. The island comprises five geological units[26], ranging in age from Pliocene to Pleistocene (0.059–3.9 Ma)[27,28], composed of silica-undersaturated and alkaline lava flows,

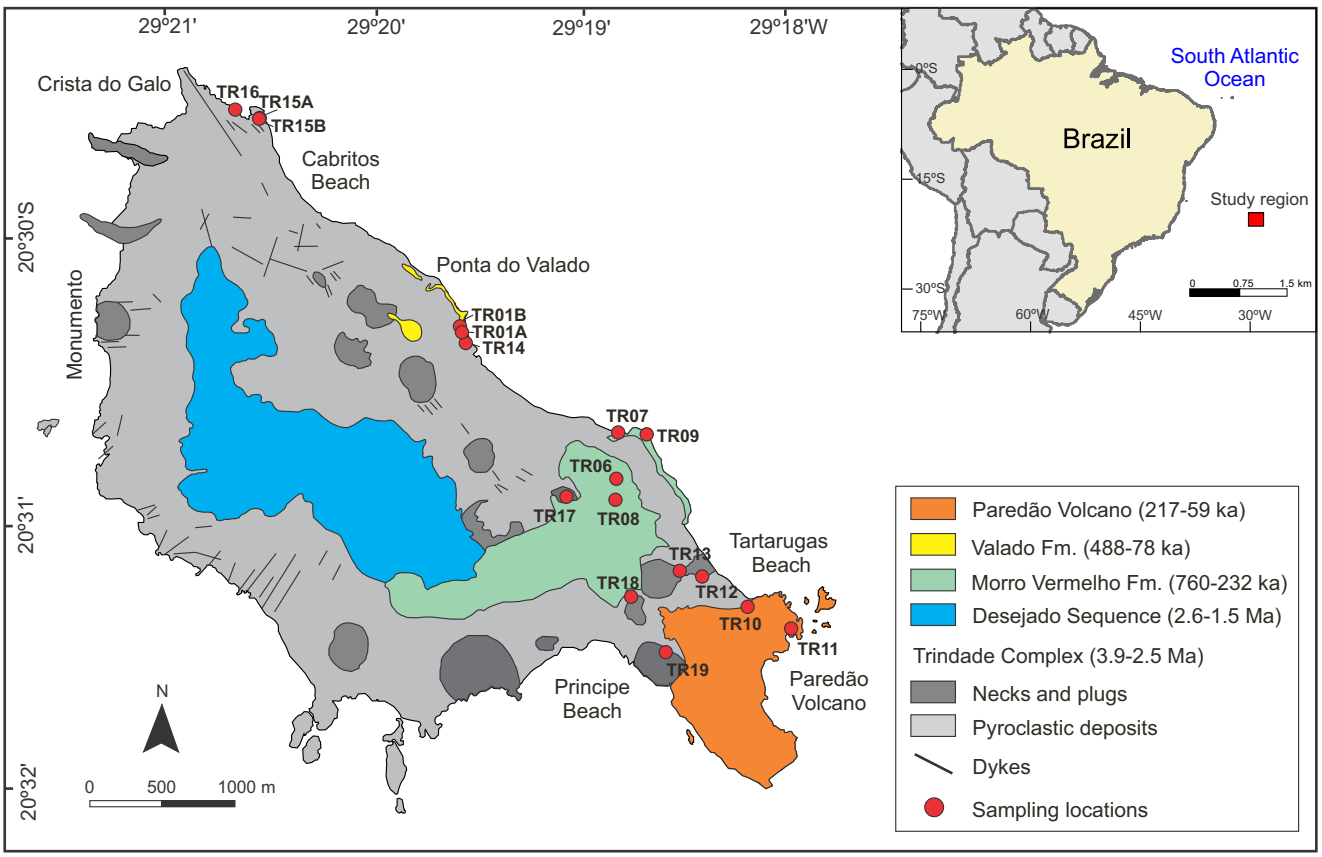

Fig. 1 | Simplified geological map of Trindade island. The red circles indicate the location of the paleomagnetic sites identified by the acronym TR (Trindade). Map adapted from[28] [Quaternary Geochronology, Volume 81, Pasqualon et al., New volcanological, ^{40}Ar/^{39}Ar dating and paleomagnetic record from Trindade Island and stratigraphic implications, 101518], Copyright (2024), with permission from Elsevier. Inset panel reprinted from[30], Copyright (2020), with permission from Elsevier. Source data are provided as a Source Data file.

https://doi.org/10.1038/s41467-024-53688-2

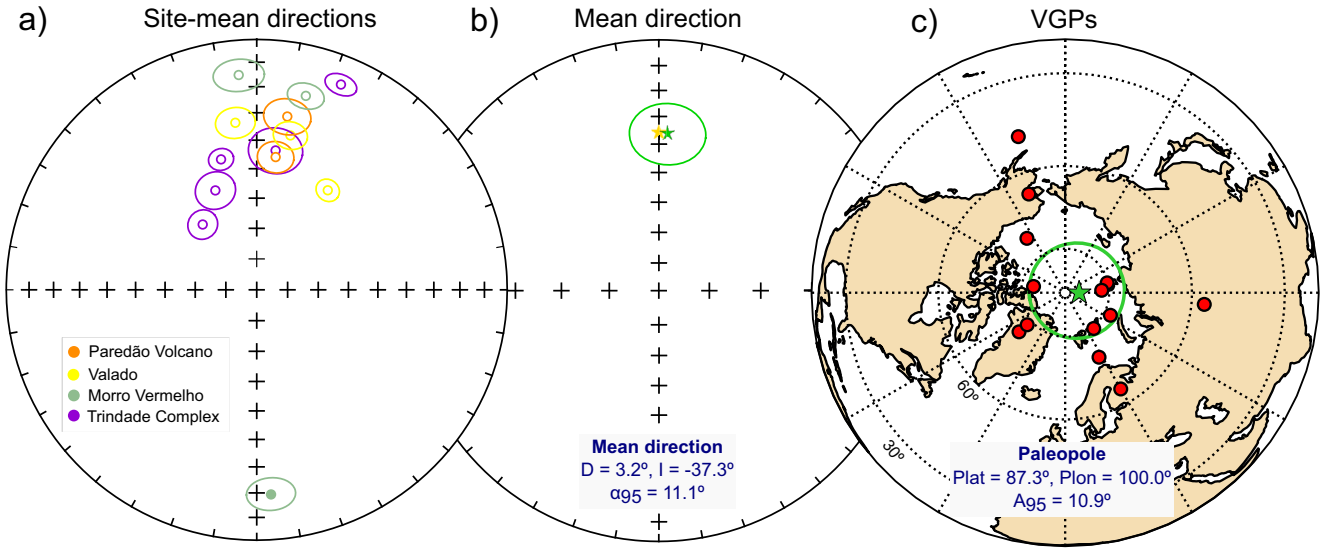

Fig. 2 | Graphical representation of paleodirectional data. a Equal area projection for normal (empty circles) and reversed (closed circle) site-level directions with values of $n \geq 5$ and $k \geq 50$. **b** Mean direction represented by green star with 95% confidence circle (α_{95}) with the values of declination (D), inclination (I). Yellow star indicates the expected GAD direction. **c** Polar stereographic map with VGP locations (red circles). The paleopole position is represented by a green star with 95% confidence circle (A_{95}) with the coordinates of the paleopole latitude (Plat) and longitude (Plon). GAD = geocentric axial dipole, VGP = virtual geomagnetic pole. Figures **a**–**c** were created using the PmagPy software package[61]. Source data are provided as a Source Data file.

pyroclastic rocks, dykes and necks[29,30] (Supplementary Information and Text S1). A field season was carried out in 2017 to collect samples from 17 paleomagnetic sites from four geological units of Trindade Island (Supplementary Figs. S2 and S3). Eight sites were sampled for the oldest unit termed Trindade Complex, of which 7 represent phonolitic necks and a thin dyke. The other nine sites correspond to a'a lava flows of the youngest units, the Morro Vermelho (4 sites), Valado (3 sites), and Paredão Volcano (2 sites) Formations. We note that the limited quantity of sampling sites is related to the difficulty in accessing the volcanic targets over the extremely rugged terrain of the island.

Alternating field (AFD) and thermal demagnetization (THD) techniques were used to determine the characteristic remanent magnetization (ChRM) components of the measured specimens (see the Methods section). Demagnetization diagrams reveal that ChRM directions from each specimen were isolated by progressive AF demagnetization from 10 to 60 mT and thermal treatments between 400 °C and 600 °C (Fig. S4). The natural remanent magnetization (NRM) was mostly cleaned at 580 °C, suggesting magnetite or low-Ti titanomagnetite as the dominant magnetic carriers as reported by a previous study[30]. A total of 119 specimens produced acceptable directions considering a maximum angular deviation MAD ≤10° as indicated by deviation angle DANG ≤5°, with linear trajectories that converge to the origin of Zijderveld[31] diagram. Among these, 79% of the specimens have values of MAD ≤5° (Supplementary Fig. S5).

Site-level directions were successfully obtained for 15 paleomagnetic sites (Supplementary Table S1) using Fisher[32] statistics. For the purpose of the PSV and TAF analysis, we also rejected two sites that do not meet the selection criteria defined by values of $k \geq 50$ and $n \geq 5$ (Fisher precision parameter and number of specimens per site, respectively), which is consistent with the current 0–10 Ma database suggested by de Oliveira et al.[25]. As addressed by some studies[25,33], the low-quality data may produce an overestimate in the VGP dispersion, which was ascertained in this study (see Supplementary Table S2). Therefore, our high-quality dataset comprises 13 paleodirectional sites, all of them with normal polarity except for site TR08 (Supplementary Table S1; Fig. 2a) from Morro Vermelho Formation. No transitional sites were recognized by employing the Vandamme[34] method or a fixed 45° cutoff angle. The mean direction calculated for $N = 13$ sites results in a declination (D) of 3.2°, inclination (I) of −37. 3°, and 95% confidence cone (α_{95}) of 11. 1° that is not statistically different at the 95% confidence level from the expected GAD direction for the studied area ($D_{GAD} = 0°$, $I_{GAD} = -37.0°$), as reported in Supplementary Table S2 and Fig. 2b.

VGPs were calculated based on the site-mean directions and their paleolocations, after performing plate motion corrections using the NNR-MORVEL56 model[35] (Supplementary Table S1). The paleopole position (Plat = 87.3°N, Plon = 100.0°E, A_{95} = 10. 9°, $N = 13$) is statistically compatible with the Earth's rotation axis within the 95% confidence interval (Supplementary Table S2; Fig. 2c). Furthermore, there is a close correspondence between the magnetic polarity of the site-mean directions and the most recent geomagnetic polarity time scale[36](Supplementary Fig. S6). At least four polarity reversals were accounted for the last 4 Myr, which is presumably long enough to average out the paleosecular variation, allowing to compute the paleopole.

VGP dispersion and inclination anomaly estimates

A VGP dispersion (S_B) was calculated with lower (S_{Bl}) and upper (S_B^u) 95% bootstrap confidence limits[37] to detect any anomalous directional variability in the studied area. These results were then compared with the global 0–10 Ma database[25] that comprises 80 high-quality studies (Fig. 3a). Using this compilation, an adapted Model G[38] (see Methods section) yielded parameters $a = 11.3^{12.9^\circ}_{9.6}$ and $b = 0.25^{0.30}_{0.20}$ (Table 1) that describe the average latitudinal pattern of PSV. As shown in Fig. 3b, the VGP dispersion for Trindade Island ($S_B = 20.6^{26.1^\circ}_{13.9}$) is remarkably higher than four other PSV studies located between latitudes 15–30°S (datasets #1, 2, 3 and 4 in Fig. 3): two are from Reunion Island[39,40] at ~ 21. 1°S ($S_B = 11.8^{13.3^\circ}_{8.8}$ and $S_B = 11.1^{12.6^\circ}_{8.7}$), and the other two are from French Polynesia[41] at 17. 7°S ($S_B = 13.6^{14.9^\circ}_{12.2}$) and Easter Island[42] at 27. 1°S ($S_B = 9.2^{11.7^\circ}_{6.1}$). However, these estimates in conjunction with our results are not significantly different from Model G fit for the 95% confidence region (blue-shaded area). These four locations are longitudinally far outside the present-day SAA region. Another PSV study conducted in the South Atlantic, on Saint Helena Island[21] (mean paleolatitude of 17. 6°S) from 8–10 Ma lava flows exhibits a pronounced dispersion (#5 in Fig. 3; $S_B = 21.3^{25.1^\circ}_{17.6}$) similar to the present work, and falls outside of the Model G curve (green triangle; Fig. 3b). Our results together with

https://doi.org/10.1038/s41467-024-53688-2

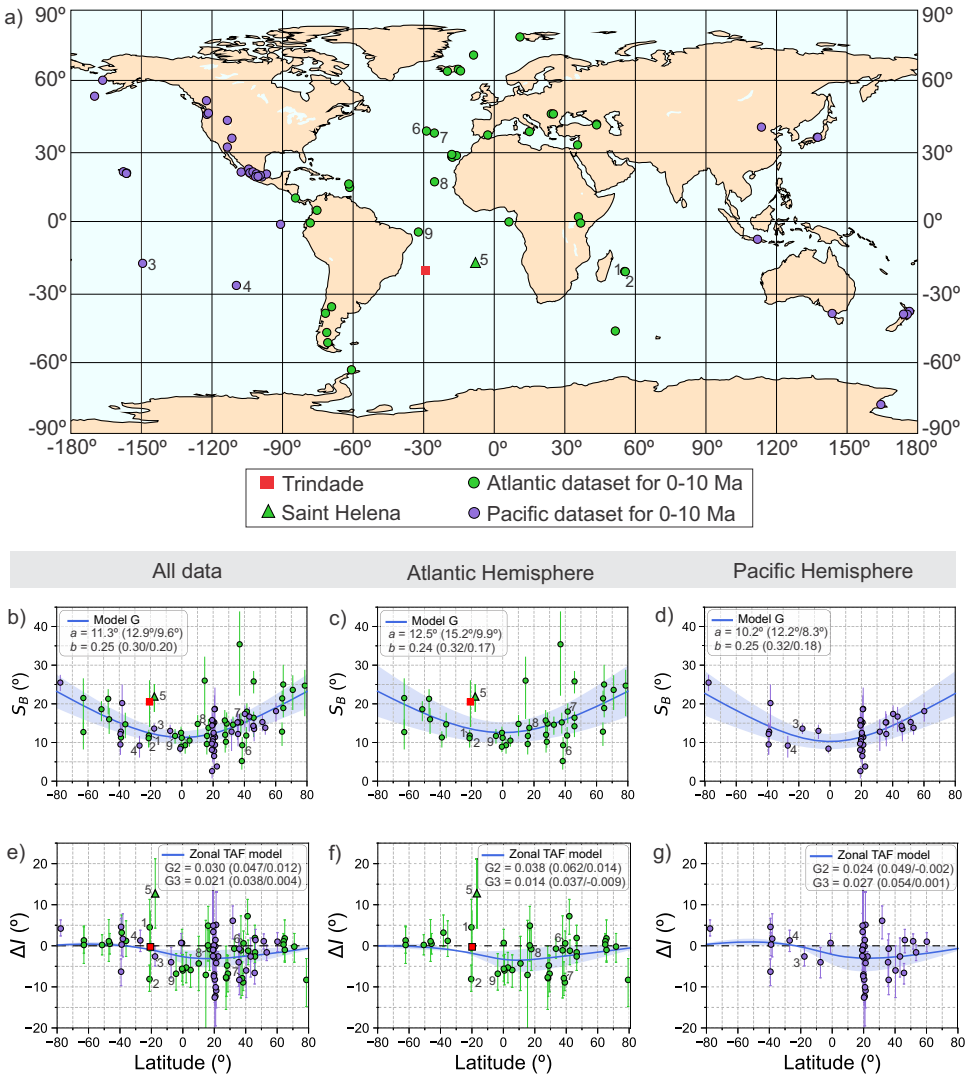

Fig. 3 | Comparison of 0–10 Ma datasets and paleomagnetic field models. **a** Location map of the 0–10 Ma database[25] and Trindade Island (red square). VGP dispersion (S_B) as a function of latitude for (**b**) all data, (**c**) Atlantic Hemisphere (−90°E to 90°E; green circles), and (**d**) Pacific Hemisphere (90°E to 270°E; purple circles). Blue lines represent the Model G[38] curves and 95% confidence intervals (blue-shaded areas). The values of the Model G *a* and *b* parameters are shown in the left panel. Latitudinal distribution of inclination anomaly (ΔI) data from this study (red square) and global 0–10 Ma dataset considering (**e**) all data, (**f**) Atlantic Hemisphere, and (**g**) Pacific Hemisphere. Blue curves denote the best-fit TAF models for each dataset, with the 95% region confidence represented by a blue-shaded area. The axial quadrupole (*G2*) and octupole (*G3*) contributions relative to the axial dipole term are shown in right panel. Numbers refer to the locations reported in the text (1,2 - Reunion Island; 3 - French Polynesia; 4 - Easter Island; 5 - Saint Helena; 6,7 - Azores; 8 - Cape Verde; 9 - Fernando de Noronha). TAF = time-averaged geomagnetic field, VGP = virtual geomagnetic pole. Source data are provided as a Source Data file.

Table 1 | Values of Model G *a* and *b* parameters, zonal quadrupole (G2) and octupole (G3) contributions, and axial dipole dominance estimated for three datasets

Dataset	*N*	*a* (u/l°)	*b* (u/l)	*G2* (u/l)	*G3* (u/l)	AD/NAD_{median}
Last 10 Ma	80	11.3 (12.9/9.6)	0.25 (0.30/0.20)	0.030 (0.047/0.012)	0.021 (0.038/0.004)	11.5 ± 6.8
Atlantic H.	41	12.5 (15.2/9.9)	0.24 (0.32/0.17)	0.038 (0.062/0.014)	0.014 (0.037/−0.009)	9.1 ± 6.3
Atlantic H.[a]	42	12.9 (15.5/10.2)	0.24 (0.32/0.16)	0.038 (0.062/0.014)	0.014 (0.037/−0.008)	8.6 ± 5.8
Pacific H.	39	10.2 (12.2/8.3)	0.25 (0.32/0.18)	0.024 (0.049/−0.002)	0.027 (0.054/0.001)	14.5 ± 9.4

N is the number of data used to determine the best-fit parameters of the PSV and TAF models. *a* and *b* are the Model G[38] parameters. *G2* and *G3* correspond to the axial quadrupole and octupole components relative to the axial dipole term. AD/NAD_{median} refers the ratio between axial dipole component and non-axial dipole components[24] with their uncertain bounds. u/l corresponds upper/lower 95% confidence bound.
H hemisphere.
[a]Dataset that includes data from Trindade Island.

those from Saint Helena suggest that the high dispersion can be connected with the anomalous PSV behavior in the South Atlantic region, persistent over the last 10 Myr. Notwithstanding, the small number of sites (N) from this study, which might influence the VGP dispersion value, it is above the minimum ($N \geq 9$) required by PSV studies[43,44]. We assert that this condition is minimized due to the rigorous selection criteria applied here to obtain high-quality paleodirectional data. Other studies were compared taking into account locations of similar longitude to Trindade Island at different latitudes. There are two PSV studies in the northern hemisphere (datasets #7 and 8 in Fig. 3) from Azores (37. 7°N, 25. 5°W) and Cape Verde (17. 0°N, 25. 4°W), with VGP dispersion values ($S_B = 15.2^{17.7^\circ}_{12.3}$ and $S_B = 13.8^{16.1^\circ}_{10.9}$, respectively) that are statistically compatible within the 95% uncertainty limits of Model G. A low estimate is found in another study in Azores (38. 6°N, 28. 2°W; #6 in Fig. 3) with $S_B = 9.3^{11.4^\circ}_{6.0}$, possibly due to the short time interval (1.9–7.8 ka) that was sampled in this location. In the southern hemisphere, a study reported east of Brazil at low latitude (Fernando de Noronha; 4. 3°S, 32. 3°W) has value of $S_B = 11.7^{13.5^\circ}_{9.7}$ (#9 in Fig. 3) consistent with Model G at the 95% confidence level. This location does not capture the enhanced long-term PSV behavior observed in this study and Saint Helena and may be associated with a border region of this anomalous field feature.

Regarding the TAF analysis, the inclination anomaly (ΔI) is determined by the deviation of the mean direction relative to the expected GAD direction (see Methods section). The low negative value of ($\Delta I = -0.3^{8.6^\circ}_{-9.2}$) from this study is not statistically significantly different from a GAD field model ($\Delta I = 0°$) as illustrated by Fig. 3e. Likewise, our result is consistent with predictions of the TAF model fitted to the global ΔI database within the 95% confidence level, with zonal quadrupole and octupole contributions of $g_0^2 = 3.0\%$ and $g_0^3 = 2.1\%$ to the axial dipole term (g_0^1), respectively (Table 1). Comparisons with studies in the 15–30°S latitude bin show differences in inclination anomaly values. There are three estimates (datasets #1, 3 and 4 in Fig. 3) from Reunion Island[39] ($\Delta I = 4.5^{11.3^\circ}_{-1.3}$), French Polynesia[41] ($\Delta I = -2.6^{-0.1^\circ}_{-4.9}$) and Easter Island[42] ($\Delta I = 1.3^{3.8^\circ}_{-1.4}$) that are in agreement with a zonal TAF model. A large negative value of $\Delta I = -8.1^{-4.7^\circ}_{-11.1}$ from Reunion Island[40] (#2 in Fig. 3) may be related to the short time span (historic) represented by the sampled lava flows covering the interval between 80–90 ka. Conversely, the high positive anomaly ($\Delta I = 12.5^{21.2^\circ}_{4.3}$) found for Saint Helena Island[21], can be associated with an anomalous geomagnetic field behavior in the region. One cannot, however, rule out the possibility that outliers are a result of additional non-axial dipole contributions to the TAF model. Through comparison with other studies of similar longitudes, we noticed that the three data from the northern hemisphere (two are from Azores ($\Delta I = 0.6^{3.6^\circ}_{-2.4}$ and $\Delta I = -7.9^{-3.9^\circ}_{-12.1}$) and one from Cape Verde ($\Delta I = -0.8^{4.5^\circ}_{-6.0}$)) and data from Fernando de Noronha ($\Delta I = -6.8^{-1.9^\circ}_{-10.8}$) for the southern hemisphere, are not significantly different at the 95% confidence limits from the 0–10 Ma TAF model.

Atlantic-Pacific hemispheric asymmetries

We extended the investigations to the whole globe in order to identify latitudinal differences in PSV behavior and zonal field structures between the Atlantic and Pacific hemispheres (separation at −90°E and 90°E) in the 0–10 Ma database (Fig. 3a). By examining the distribution of S_B data, the Atlantic hemisphere has a higher amount of data (22 out of 42) that falls above the Model G fit compared to the Pacific hemisphere (13 out of 39; Fig. 3b), thereby corroborating a previous observation[21]. Also, differences in the latitudinal pattern of PSV are found for Model G curves fitted to S_B datasets for each hemisphere separately (Fig. 3c, d; Table 1). Atlantic data produce weak latitudinal dependence in the VGP dispersion curve (caused by elevated equatorial VGP dispersion) with Model G parameters $a = 12.5^{15.5^\circ}_{9.9}$ and $b = 0.24^{0.32}_{0.17}$ that are, respectively, higher and slightly lower than the Pacific hemisphere ($a = 10.2^{12.2^\circ}_{8.3}$ and $b = 0.25^{0.32}_{0.18}$). Our results suggest a high (low) geomagnetic variability for the Atlantic (Pacific) sector spanning the last 10 Myr.

Atlantic-Pacific hemispheric asymmetries are also observed from the best-fit two parameter zonal TAF models using the inclination anomaly estimates for the past 10 Myr (Fig. 3f, g). In general, Atlantic data reveal a greater number of negative anomalies (> −5°) in low- to mid-northern latitudes in relation to the Pacific hemisphere (Fig. 3e). The values of quadrupole ($G2 = g_0^2/g_0^1 = 3.8\%$) and octupole ($G3 = g_0^3/g_0^1 = 1.4\%$) components for the Atlantic and Pacific ($G2 = 2.4\%$ and $G3 = 2.7\%$) are statistically indistinguishable at the 95% confidence level (Table 1). The prominent value of the G3 term for the Pacific sector is usually ascribed to the presence of positive anomalies in mid- to high-southern latitudes[23] (Fig. 3g). But in this latitude band, the data coverage is sparse and paleomagnetic constrains are derived only from New Zealand[45–47], Australia[48] and Antarctica[49]. Further data are needed to improve the spatial resolution of the average field structure in this sector. Interestingly, Model LN3[4] designed to examine the non-zonal TAF features for the 0–5 Ma period shows positive ΔI over the southwestern Pacific and some regions of Antarctica. These observations suggest that regional differences of non-GAD field structures may be persistent over the multimillion year periods.

Discussion

Long-lived non-dipole field in the South Atlantic

Recent studies[24,50] have offered insights on the average paleomagnetic field morphology based on paleosecular variation data. Biggin et al.[24] postulated a power law relationship between Model G a parameter and the average axial dipole, which was estimated from a series of geodynamo simulations differentiated by input parameters and physical properties. Here, we determined the median ratios of axial dipole (AD) to non-axial dipole (NAD) components (see Methods section) to assess the degree of average field dipolarity in the Atlantic and Pacific hemispheres using the Model G a values. The AD/NAD_{median} ratio determined for the Atlantic region (9.1 ± 6.3) is lower than the Pacific (14.5 ± 9.4). When Trindade Island data are incorporated into the Model G fit, the AD/NAD_{median} value for the Atlantic Hemisphere decreases (see Table 1). These findings provide compelling evidence for a long-term hemispheric field asymmetry, suggesting a weaker average dipole dominance (i.e., strong NAD effects) in the Atlantic with respect to the Pacific hemisphere, and could be linked to enhanced PSV activity in the former as previously observed in geomagnetic field models for the present, centennial and millennial time scales[3,5,19]. The enhanced geomagnetic variability detected in the South Atlantic region for the past 10 Myr (Fig. 3) may be attributed to heterogeneous boundary conditions at the top as well as at the bottom of the outer core. Tarduno et al.[8] suggests that geomagnetic flux patches are recurrent below the South Atlantic region linked to African LLSVP. Consequently, it reflects an area of preferential magnetic flux expulsion of toroidal field lines at the top of the core that forms pairs of normal and reversed flux patches at the CMB[51], producing large departures from dipolarity. Alternatively, a bottom-up control of the outer core dynamics associated with the Earth's inner core growth can produce large secular variation hemisphericity between the Atlantic and Pacific[52]. We further discuss the understanding of Earth's deep dynamics and its relation to PSV in the next subsection.

VGP dispersion is highly dependent on latitude over historical time[53]. An analysis[25] of VGP dispersion data separately for each hemisphere using the COV-OBS geomagnetic field model[54] between 1840 and 2020, shows a marked north-south hemispheric asymmetry for more recent times (Fig. 4a). The contribution of specific non-zonal harmonic terms can result in significant changes in the shape of the VGP dispersion curve, as pointed out by historical field observations[25,53]. However, the strength and spatial configuration of geomagnetic flux patches can lead to more complex field structures and, consequently, PSV changes with geographic latitude. To evaluate

https://doi.org/10.1038/s41467-024-53688-2

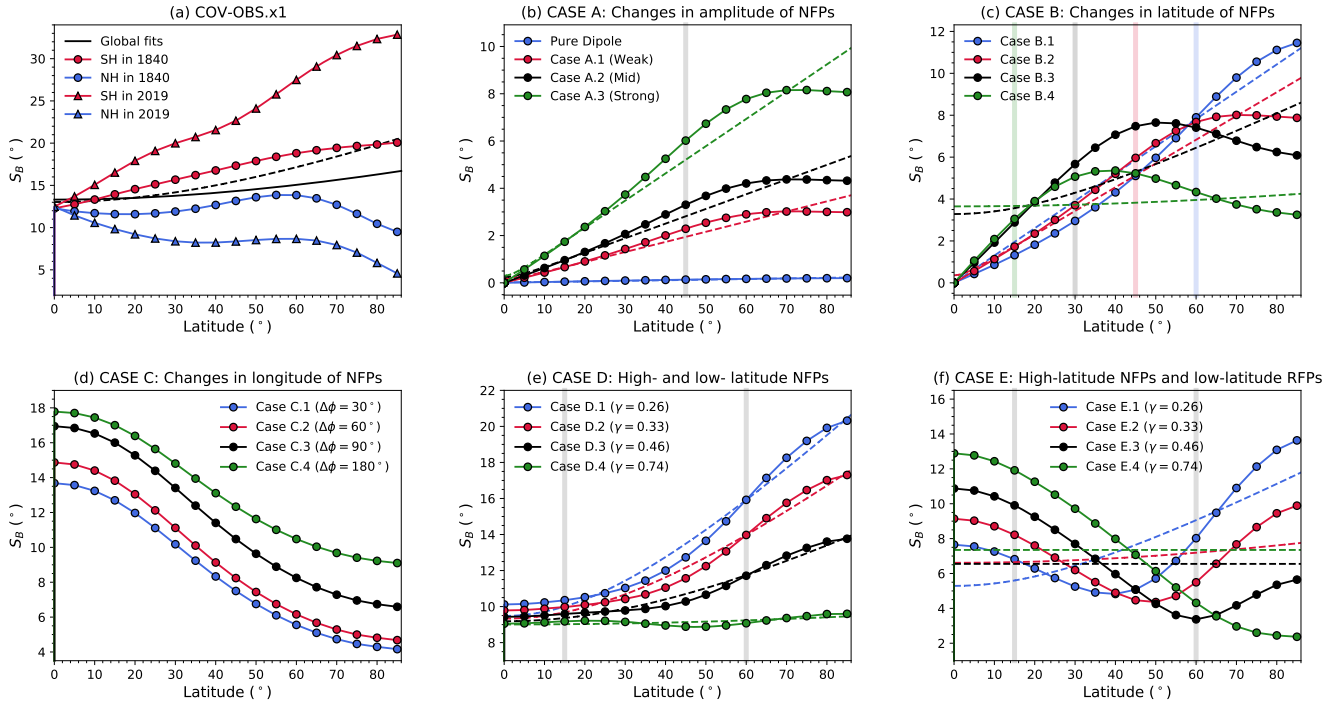

Fig. 4 | Angular dispersion curves of data obtained from synthetic geomagnetic field models. VGP dispersion (S_B) as a function of latitude (**a**) for a snapshot of a geomagnetic field model[54] separately for the northern hemisphere (NH) and southern hemisphere (SH); and (**b**–**f**) for several idealized CMB radial magnetic field scenarios. Thick shaded lines denotes the latitudes of the center of the synthetic flux patches (gray if fixed, colored if cases are latitudinal dependent). Dashed lines denote the correspondent Model G curves. $\Delta\phi$ denotes the distance in longitude between geomagnetic flux patches and γ is the ratio (in absolute value) between the amplitude of the lower latitude patch over the higher. NFPs = normal flux patches. RFPs = reversed flux patches, VGP = virtual geomagnetic pole. Source data are provided as a Source Data file.

the latitudinal behavior of VGP dispersion under the influence of RFPs and normal flux patches (NFPs), we propose a series of five synthetic scenarios at the CMB, taking into account changes in the location and intensity of geomagnetic flux patches (cases A to E reported in Fig. 4b–f). These models were constructed from a background axial dipole field, in which equatorially anti-symmetric flux patches are superimposed (see Methods section). Case A shows changes in amplitude of two NFPs centered at latitudes 45°, one in each hemisphere (Fig. 4b). The latitudinal dependence of S_B increases with the intensity of NFPs. Case A also indicates a latitude-invariant dispersion of VGPs for a pure dipole field and validates our numerical approach. As in Case A, Case B also shows a pair of NFPs, but their locations are situated at different latitudes (Fig. 4c). The VGP dispersion tends to increase from the equator to the pole, with a bump that varies latitudinally nearly 20° higher in latitude than the location of the NFPs. Case C shows two NFPs in the same latitude along the equator with changes in the longitudinal distance ($\Delta\phi$) between them (Fig. 4d). In general, the S_B estimates decrease from equator to the pole with higher values for all latitudes with $\Delta\phi$ increases. Case D has two pairs of NFPs (Fig. 4e), one pair is located at low latitude (15°) and the other at high latitude (60°). The pattern of VGP scatter is determined by the ratio between the amplitude of lower and higher latitude patches (indicated by γ). The latitudinal dependence of S_B increases with decreasing γ values. Finally, Case E shows two NFPs and two RFPs located, respectively, at high and low latitudes (Fig. 4f). Significant changes in the shapes of the VGP dispersion curves are observed for different values of γ. Among the scenarios examined, case D with γ = 0.26 is the one that most closely approximates the latitudinal pattern of PSV observed for the last 10 Myr. Our results suggest that the geomagnetic field has a clear influence from NFPs (linked with its position and intensification at the CMB) in general over the past 10 Myr. Moreover, the present-day geomagnetic field presents a low-latitude (slightly southern) belt of normal flux patches at the CMB[7] which produces comparable low-latitude S_B values in the Southern Hemisphere (Fig. 4a) to our finding in Trindade Island. Alternatively, according to Case E, RFPs also create a peak in the VGP dispersion and can not be discarded as the source of recurrent high VGP dispersion estimates found in data from Saint Helena Island[21] and in this study. Hence our synthetic results can also be interpreted as indicative of RPFs in the South Atlantic Ocean which may be responsible for the recurrence of SAA like features at ancient epochs of Earth's magnetic field[17,20].

A top-down or bottom-up control on the long-term field behavior?

Lateral heterogeneous boundaries influence the outer core flow dynamics, and consequently the geomagnetic field and its time-dependence[52,55]. In the outer boundary, the lowermost mantle, stable over several hundred millions of years[56], modulates the outgoing heat from the core to the mantle. Hence lowermost mantle lateral heterogeneities may produce persistent regional upwelling and downwelling flow structures[18,57] resulting in geomagnetic field structures top-down controlled. Tarduno et al.[8] proposed that core fluid upwelling under the eastern edge of the African LLSVP could be responsible for the appearance of pairs of RFPs and NFPs at the CMB, hence producing recurrently strong non-dipole field at the CMB and an anomalously weak intensity field at the Earth's surface (the SAA). Recent geomagnetic field reconstructions[13–15] and new archeointensity records[8–10] have suggested that SAA-like structures are recurrent over time. A long-term SAA longevity hypothesis has been supported by low average paleointensities and high VGP dispersion in the South Atlantic region from Tristan da Cunha[22] and Saint Helena[20,21] islands during Late Pleistocene (46–90 ka) and Late Miocene (8–10 Ma), respectively. Our paleomagnetic record in Trindade Island expands these records towards west, close to the continental margin of Brazil and also in time covering the Pliocene-Pleistocene interval (Fig. 3). According to our idealized geomagnetic field scenarios and synthetic VGP dispersion

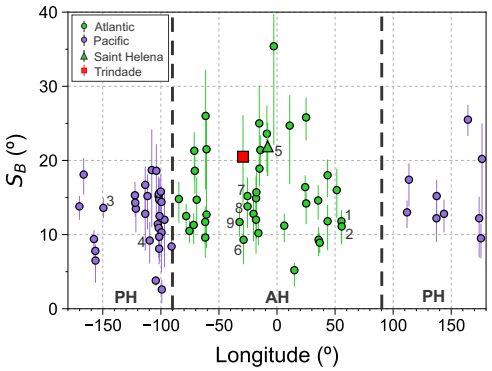

Fig. 5 | VGP dispersion (S_B) as a function of longitude. The green (purple) circles represent Atlantic (Pacific) data. Numbers refer to the locations reported in the text (1,2 - Reunion Island; 3 - French Polynesia; 4 - Easter Island; 5 - Saint Helena; 6,7 - Azores; 8 - Cape Verde; 9 - Fernando de Noronha). VGP = virtual geomagnetic pole, PH = Pacific Hemisphere, AH = Atlantic Hemisphere.

curves, regional differences in the 0–10 Ma paleomagnetic field can be attributed to the recurrent presence of intense low-latitude flux patches of either reversed or normal polarity hence not necessarily linked to persistent anomalous weak field at Earth's surface (Fig. 4).

Records of the Holocene[19] and Pleistocene[16] epochs show an Atlantic-Pacific dichotomy for the PSV index, though the statistical robustness of these results has been questioned[58]. Here, we found over at least the past 10 Myr, an Atlantic-Pacific dichotomy in our paleomagnetic secular variation models (Figs. 3 and 5). Using numerical dynamo simulations that account for lateral heterogeneities of the lowermost mantle, Mound and Davies[58] investigated if thermal structural differences would produce the hemispheric SV asymmetry. No statistically significant preference for a given hemisphere in terms of temporal variability was found in their models time-averages. Conversely, numerical dynamo simulations with bottom-up control over outer core dynamics by the Earth's inner core reproduced the Atlantic-Pacific SV dichotomy[52]. Aubert et al.[52] proposed a dominant bottom-up mechanism driving the Earth's magnetic field secular variation, contrasting with previous mantle-driven hypotheses. They highlighted the inner core's crucial role, particularly in localizing the magnetic variations beneath the Atlantic, attributing longitudinal localization to thermochemical interactions between the inner and outer core and latitudinal localization to gravitational coupling between the inner core and mantle. They suggested that while the mantle's influence on the SV is secondary, it collaborates with the inner core to maintain the low secular variation in the Pacific. Our results corroborate for a more time-dependent Atlantic than Pacific hemisphere over the past 10 Myr. Following Aubert et al.[52], it may suggest a stronger bottom-up than the top-down control of the geodynamo temporal variability during the past 10 Myr. However, the morphology of the geomagnetic field, in particular the persistent presence of two intense high-latitude NFPs at each hemisphere, is likely controlled by the lower mantle thermal heterogeneity[57,59,60].

Methods

Paleomagnetic measurements and data analysis

Paleodirectional experiments were conducted in a magnetically shielded room at the Paleomagnetism Laboratory of the University of São Paulo (USPMag). A minimum of five specimens from each site (200 specimens in total) were subjected to alternating-field (AFD) or thermal demagnetization (THD), using an ASC-TD48 thermal demagnetizer oven, a LDA5 AF demagnetizer (AGICO), 2G cryogenic magnetometer equipped with a RAPID (Rock and Paleomagnetism Instrument Development) system, and a JR-6A spinner magnetometer (AGICO). AFD measurements were performed on 143 specimens in 18 progressive steps from 2 to 100 mT. THD were carried out for the 57 remaining specimens in 17 steps from room temperature to 600° C or complete removal of the NRM. Using the PmagPy Demag Gui program[61], the ChRM directions at the specimen level were obtained through principal component analysis (PCA)[62]. At least five demagnetization data which decayed toward the origin of the Zijderveld[31] plots were considered for ChRM estimation, with values of maximum angular deviation MAD[62]≤10° and deviation angle DANG[63]≤5°. Site-mean directions were determined using Fisher[32] statistics. Following de Oliveira et al.[25] criteria, a minimum number of five specimens per site ($n \geq 5$) with a Fisher precision parameter $k \geq 50$ were considered for PSV and TAF investigations.

Estimate of VGP dispersion and Model G fits

The variability of paleodirectional data was measured by the between-site VGP dispersion (S_B) from N sites using the following equation[33]:

$$S_B = \sqrt{\frac{1}{N-1}\sum_{i=1}^{N}\left(\Delta_i^2 - \frac{{S_{w_i}}^2}{n_i}\right)}, \quad (1)$$

where Δ_i refers to the angular deviation of the ith VGP from the paleomagnetic pole (mean VGP position), n is the number of specimens at site level, and $S_{w_i} = 81/K_i$ is the within-site VGP disperson. With the known values of the Fisher precision parameter (k_i) of site-mean direction and its paleolatitude (λ_i), K_i is calculated as:

$$K_i = \frac{8k_i}{5 + 18\sin^2\lambda_i + 9\sin^4\lambda_i}. \quad (2)$$

Model G[38] was used for statistically assessing the latitudinal behavior of S_B data using the current 0–10 Ma database[25] including our results. This model describes the shape of the VGP scatter curve taking into account two parameters a and b:

$$S(\lambda) = \sqrt{a^2 + (b\lambda)^2}, \quad (3)$$

where a and b are associated respectively with the symmetric an antisymmetric geodynamo families about the equator. These two parameters were determined by the non-linear least squares fitting for a given S_B dataset through a *Python* algorithm (within the *scipy.optimize.leastsq* package) that uses the Levenberg–Marquardt[64] method.

Estimate of ancient axial dipole dominance

A power-law relationship between Model G a parameter and the median axial dipole (AD) dominance was recently proposed[24] from numerical geodynamo simulations and validated by observational geomagnetic field models at different timescales. It provides useful insights into the paleofield morphology based on VGP dispersion data. The estimate of the degree of AD dominance is given by:

$$\log(AD/NAD_{median}) = k_1 \log a + k_2. \quad (4)$$

The term AD/NAD_{median} denotes the ratio of AD component to the non-axial dipole (NAD) components; k_1 (= − 2.26 ± 0.13) and k_2 (= 3.44 ± 0.16) are constants that were inferred through linear least square regression in logarithmic scale. We applied the Eq. (4) to ascertain whether there are regional morphological differences between the Atlantic and Pacific hemispheres for PSV models spanning the last 10 Myr.

Estimate of inclination anomaly and zonal TAF models

A statistical approach used in investigations of the time-averaged field geometry is the inclination anomaly (ΔI), which is defined by the difference between Fisher[32] mean inclination (I_{mean}) and the inclination

expected from the GAD model (I_{GAD}), as follows[65]:

$$\Delta I = I_{mean} - I_{GAD}, \quad (5)$$

where I_{GAD} is calculated from the mean latitude ($\bar{\lambda}$) for a dataset, expressed by:

$$I_{GAD} = \tan^{-1}(2\tan\bar{\lambda}). \quad (6)$$

We evaluated the paleofield latitudinal structure based on ΔI estimates obtained from this study combined with the 0–10 Ma database. Zonal TAF models were designed from the relation between axial quadrupole (g_0^2) and octupole (g_0^3) components with the axial dipole (g_0^1), according to a predicted model for observed inclination (I_{OBS}) in function of colatitude θ (90° − λ), given by[66]:

$$\tan I_{OBS} = \frac{2\cos\theta + G2\left(\frac{9}{2}\cos^2\theta - \frac{3}{2}\right) + G3\left(10\cos^3\theta - 6\cos\theta\right)}{\sin\theta + G2(3\cos\theta\sin\theta) + G3\left(\frac{15}{2}\cos^2\theta\sin\theta - \frac{3}{2}\sin\theta\right)}. \quad (7)$$

Using Eqs. (5) to (7), the quadrupole $G2 = (g_0^2/g_0^1)$ and the octupole $G3 = (g_0^3/g_0^1)$ terms were determined by the best-fit curve for the ΔI datasets using the Levenberg–Marquardt[64] method.

Idealized geomagnetic field scenarios and synthetic VGP dispersion curves

Synthetic radial magnetic fields were built from a background axial dipole field B_r^{ad} on which equatorially anti-symmetric flux patches are superimposed[6,10,67]. The background field defines the polarity of the total field, whereas the actual dipole moment is given by the sum of the background dipole and the patches. Though patches are of much smaller spatial scale than the axial dipole, their latitudinal position and polarity (normal or reversed) greatly affects the axial dipole moment[68]. We use an anisotropic 2D-Gaussian to model the radial field of a synthetic intense magnetic flux patch[67]. For simplicity, we set the patches' orientation γ to zero. Under those conditions, each patch is defined by the Gaussian:

$$B_r^P = A_b \exp\left(\frac{(\phi - \phi_b)}{2\sigma_\phi^2} + \frac{(\theta - \theta_b)}{2\sigma_\theta^2}\right), \quad (8)$$

where ϕ and θ are longitude and co-latitude, respectively, ϕ_b and θ_b are the patch center coordinates, and A_b is the patch amplitude. σ_ϕ and σ_θ represent the distance over which the B_r^P peak decays from A_b to $A_b/3$ in the azimuthal and meridional directions, respectively. Our choice of parameters roughly mimics values of the historical era[67]. The global synthetic field B_r^{Syn} is given by the sum of the background axial dipole field and the Gaussian patches

$$B_r^{Syn} = B_r^{ad} + \sum_i (B_r^P)_i, \quad (9)$$

where i denotes summation over multiple patches. We set a pair of patches with opposite signs but same amplitudes and sizes, such that $\int_S B_r^{Syn} dS = 0$, where S denotes the entire CMB surface. Maps of idealized scenarios D.4 and E.4 are found in Supplementary Information.

We then evaluated the equivalent VGP dispersion for a series of idealized radial field models at the core-mantle boundary. We started by using kernels analysis[6,7,10,69,70] to project B_r^{Syn} upwards to the Earth's surface, thus allowing the determination of the inclination and declination of the field. Next, we computed distributions of dispersion data for each 5° latitude band, with 5° longitude spacing[25]. Note that on the spherical shell, the latter approach means better sampling at higher latitudes than the lower latitudes. However, our zonal averaged models are weakly affected. The 5° spacing is short enough scale to capture longitudinal changes at the equator even for more complex field than our synthetic fields, for instance the present-day field[25,38]. Finally, equivalent VGP dispersion curves (S_B) as a function of latitude were built.

Data availability

All paleomagnetic data generated or analyzed in this study are available in the supplementary information file and the MagIC database at https://earthref.org/MagIC/20016. Source data are provided in this paper. Source data are provided with this paper.

Code availability

The code used to perform the analyses are available from the corresponding author upon request.

References

1. Heirtzler, J. The future of the South Atlantic Anomaly and implications for radiation damage in space. *J. Atmos. Sol. Terr. Phys.* **64**, 1701–1708 (2002).
2. Hulot, G., Finlay, C. C., Constable, C. G., Olsen, N. & Mandea, M. The magnetic field of Planet Earth. *Space Sci. Rev.* **152**, 159–222 (2010).
3. Constable, C. G., Korte, M. & Panovska, S. Persistent high paleosecular variation activity in southern hemisphere for at least 10 000 years. *Earth Planet. Sci. Lett.* **453**, 78–86 (2016).
4. Cromwell, G., Johnson, C. L., Tauxe, L., Constable, C. G. & Jarboe, N. A. PSV10: A global data set for 0-10 Ma time-averaged field and paleosecular variation studies. *Geochem. Geophys. Geosystems* **19**, 1533–1558 (2018).
5. Panovska, S., Constable, C. G. & Korte, M. Extending global continuous geomagnetic field reconstructions on timescales beyond human civilization. *Geochem. Geophys. Geosystems* **19**, 4757–4772 (2018).
6. Terra-Nova, F., Amit, H., Hartmann, G. A., Trindade, R. I. F. & Pinheiro, K. J. Relating the South Atlantic Anomaly and geomagnetic flux patches. *Phys. Earth Planet. Inter.* **266**, 39–53 (2017).
7. Finlay, C. C. et al. The CHAOS-7 geomagnetic field model and observed changes in the South Atlantic Anomaly. *Earth, Planets Space* **72**, 1–31 (2020).
8. Tarduno, J. A. et al. Antiquity of the South Atlantic Anomaly and evidence for top-down control on the geodynamo. *Nat. Commun.* **6**, 7865 (2015).
9. Hare, V. J. et al. New archeomagnetic directional records from Iron Age southern Africa (ca. 425-1550 CE) and implications for the South Atlantic Anomaly. *Geophys. Res. Lett.* **45**, 1361–1369 (2018).
10. Trindade, R. I. F. et al. Speleothem record of geomagnetic South Atlantic Anomaly recurrence. *Proc. Natl Acad. Sci.* **115**, 13198–13203 (2018).
11. Jaqueto, P. et al. Stalagmite paleomagnetic record of a quiet mid-to-late Holocene field activity in Central South America. *Nat. Commun.* **13**, 1349 (2022).
12. Lopes, C. T. et al. Late holocene paleosecular variation and relative paleointensity records from Lagoa dos Patos (southern Brazil). *Phys. Earth Planet. Inter.* **332**, 106935 (2022).
13. Campuzano, S. A., Gomez-Paccard, M., Pavon-Carrasco, F. J. & Osete, M. L. Emergence and evolution of the South Atlantic Anomaly revealed by the new paleomagnetic reconstruction SHAWQ2k. *Earth Planet. Sci. Lett.* **512**, 17–26 (2019).
14. Nilsson, A., Suttie, N., Stoner, J. S. & Muscheler, R. Recurrent ancient geomagnetic field anomalies shed light on future evolution of the South Atlantic Anomaly. *Proc. Natl Acad. Sci.* **119**, e2200749119 (2022).
15. Brown, M., Korte, M., Holme, R., Wardinski, I. & Gunnarson, S. Earth's magnetic field is probably not reversing. *Proc. Natl Acad. Sci.* **115**, 5111–5116 (2018).

16. Panovska, S., Korte, M. & Constable, C. G. One hundred thousand years of geomagnetic field evolution. *Rev. Geophys.* **57**, 1289–1337 (2019).
17. Engbers, Y., Holme, R. & Biggin, A. Miocene time-averaged geomagnetic field model suggests long-lived mantle control and recurring structure in the South Atlantic. *Earth Planet. Sci. Lett.* **626**, 118535 (2024).
18. Terra-Nova, F., Amit, H. & Choblet, G. Preferred locations of weak surface field in numerical dynamos with heterogeneous core-mantle boundary heat flux: consequences for the South Atlantic Anomaly. *Geophys. J. Int.* **217**, 1179–1199 (2019).
19. Panovska, S. & Constable, C. G. An activity index for geomagnetic paleosecular variation, excursions, and reversals. *Geochem. Geophys. Geosyst.* **18**, 1366–1375 (2017).
20. Engbers, Y. A., Grappone, J. M., Mark, D. F. & Biggin, A. J. Low paleointensities and Ar/Ar ages from Saint Helena provide evidence for recurring magnetic field weaknesses in the South Atlantic. *J. Geophys. Res. Solid Earth* **127**, e2021JB023358 (2022).
21. Engbers, Y. A., Biggin, A. J. & Bono, R. K. Elevated paleomagnetic dispersion at Saint Helena suggests long-lived anomalous behavior in the South Atlantic. Proc. *Natl Acad. Sci.* **117**, 1825818263 (2020).
22. Shah, J. et al. Palaeomagnetic evidence for the persistence or recurrence of geomagnetic main field anomalies in the South Atlantic. *Earth Planet. Sci. Lett.* **441**, 113–124 (2016).
23. Johnson, C. L., & McFadden, P. L., *The time-averaged field and paleosecular variation*, vol. 5, 385-414 (Elsevier, Oxford, 2015).
24. Biggin, A. J. et al. Quantitative estimates of average geomagnetic axial dipole dominance in deep geological time. *Nat. Commun.* **11**, 1–9 (2020).
25. de Oliveira, W. P. et al. Paleosecular variation and the time-averaged geomagnetic field since 10 Ma. *Geochem. Geophys. Geosyst.* **22**, 1–23 (2021).
26. Almeida, F. F. M., *Geologia e petrologia da Ilha da Trindade* (Serviço Gráfico do Instituto Brasileiro de Geografia e Estatística, 1961).
27. Pires, G. L. C. et al. New $^{40}Ar/^{39}Ar$ ages and revised $^{40}K/^{40}Ar^{*}$ data from nephelinitic-phonolitic volcanic successions of the Trindade Island (South Atlantic Ocean). *J. Volcanol. Geotherm. Res.* **327**, 531–538 (2016).
28. Pasqualon, N. G. et al. New volcanological, $^{40}Ar/^{39}Ar$ dating and paleomagnetic record from Trindade Island and stratigraphic implications. *Quat. Geochronol.* **81**, 101518 (2024).
29. Pasqualon, N. G., de Lima, E. F., dos Santos Scherer, C. M., Rossetti, Ld. M. M. & da Luz, F. R. Lithofacies association and stratigraphy of the Paredão volcano, Trindade Island, Brazil. *J. Volcanol. Geotherm. Res.* **380**, 48–63 (2019).
30. Pasqualon, N. G. et al. Emplacement dynamics of alkaline volcanic and subvolcanic rocks in Trindade Island, Brazil. *J. Volcanol. Geotherm. Res.* **406**, 107078 (2020).
31. Zijderveld, J. D. A. *AC demagnetization of rocks: Analysis of results*, 254–286 (Elsevier, 1967).
32. Fisher, R. A. Dispersion on a sphere. *Proc. R. Soc. Lond.* **A217**, 295–305 (1953).
33. Biggin, A. J., Van Hinsbergen, D. J. J., Langereis, C. G., Straathof, G. B. & Deenen, M. H. L. Geomagnetic secular variation in the Cretaceous Normal Superchron and in the Jurassic. *Phys. Earth Planet. Inter.* **169**, 3–19 (2008).
34. Vandamme, D. A new method to determine paleosecular variation. *Phys. Earth Planet. Inter.* **85**, 131–142 (1994).
35. Argus, D. F., Gordon, R. G. & DeMets, C. Geologically current motion of 56 plates relative to the no-net-rotation reference frame. *Geochem. Geophys. Geosyst.* **12**, 1–13 (2011).
36. Ogg, J. G., Geomagnetic polarity time scale. In *Geologic time scale 2020*, 159–192 (Elsevier, 2020).
37. Tibshirani, R. J. & Efron, B. An introduction to the bootstrap. *Monogr. Stat. Appl. Probab.* **57**, 1–436 (1993).
38. McFadden, P. L., Merrill, R. T. & McElhinny, M. W. Dipole/quadrupole family modeling of paleosecular variation. *J. Geophys. Res. Solid Earth* **93**, 11583–11588 (1988).
39. Raïs, A., Laj, C., Surmont, J., Gillot, P.-Y. & Guillou, H. Geomagnetic field intensity between 70 000 and 130 000 years BP from a volcanic sequence on La Reunion, Indian Ocean. *Earth Planet. Sci. Lett.* **140**, 173–189 (1996).
40. Chauvin, A., Gillot, P.-Y. & Bonhommet, N. Paleointensity of the Earth's magnetic field recorded by two late Quaternary volcanic sequences at the island of La Reunion (Indian Ocean). *J. Geophys. Res. Solid Earth* **96**, 1981–2006 (1991).
41. Yamamoto, Y. et al. Geomagnetic paleosecular variation for the past 5 Ma in the Society Islands, French Polynesia. *Earth, Planets Space* **54**, 797–802 (2002).
42. Miki, M. et al. Geomagnetic paleosecular variation in Easter Island, the southeast Pacific. *Phys. Earth Planet. Inter.* **106**, 93–101 (1998).
43. Doubrovine, P. V. et al. Latitude dependence of geomagnetic paleosecular variation and its relation to the frequency of magnetic reversals: Observations from the Cretaceous and Jurassic. *Geochem. Geophys. Geosyst.* **20**, 1240–1279 (2019).
44. Handford, B. T., Biggin, A. J., Haldan, M. M. & Langereis, C. G. Analyzing Triassic and Permian Geomagnetic Paleosecular Variation and the Implications for Ancient Field Morphology. *Geochem. Geophys. Geosyst.* **22**, 1–22 (2021).
45. Tanaka, H., Kawamura, K., Nagao, K. & Houghton, B. F. K-Ar ages and paleosecular variation of direction and intensity from Quaternary lava sequences in the Ruapehu Volcano, New Zealand. *J. Geomagn. Geoelectr.* **49**, 587–599 (1997).
46. Lerner, G. A., Cronin, S. J., Turner, G. M. & Rowe, M. C. Paleomagnetic determination of the age and properties of the 1780-1800 AD dome effusion/collapse episode of Mt. Taranaki, New Zealand. *Bull. Volcanol.* **81**, 1–20 (2019).
47. Tanaka, H., Komuro, N. & Turner, G. M. Palaeosecular variation for 0.1-21 ka from the Okataina Volcanic Centre, New Zealand. *Earth Planets Space* **61**, 213–225 (2009).
48. Opdyke, N. D. & Musgrave, R. Paleomagnetic results from the Newer Volcanics of Victoria: Contribution to the time averaged field initiative. *Geochem. Geophys. Geosyst.* **5**, 1–10 (2004).
49. Lawrence, K. P. et al. Paleomagnetic field properties at high southern latitude. *Geochem. Geophys. Geosyst.* **10**, 1–27 (2009).
50. Meduri, D. G. et al. Numerical dynamo simulations reproduce paleomagnetic field behavior. *Geophys. Res. Lett.* **48**, 1–10 (2021).
51. Bloxham, J. The expulsion of magnetic flux from the Earth's core. *Geophys. J. Int.* **87**, 669–678 (1986).
52. Aubert, J., Finlay, C. C. & Fournier, A. Bottom-up control of geomagnetic secular variation by the Earth's inner core. *Nature* **502**, 219–223 (2013).
53. Hulot, G. & Gallet, Y. On the interpretation of virtual geomagnetic pole (VGP) scatter curves. *Phys. Earth Planet. Inter.* **95**, 37–53 (1996).
54. Gillet, N., Barrois, O. & Finlay, C. C. Stochastic forecasting of the geomagnetic field from the COV-OBS.x1 geomagnetic field model, and candidate models for IGRF-12. *Earth Planets Space* **67**, 1–14 (2015).
55. Aubert, J., Amit, H. & Hulot, G. Detecting thermal boundary control in surface flows from numerical dynamos. *Phys. Earth Planet. Inter.* **160**, 143–156 (2007).
56. McNamara, A. K. A review of large low shear velocity provinces and ultra-low velocity zones. *Tectonophysics* **760**, 199–220 (2019).
57. Gubbins, D., Willis, A. P. & Sreenivasan, B. Correlation of Earth's magnetic field with lower mantle thermal and seismic structure. *Phys. Earth Planet. Inter.* **162**, 256–260 (2007).
58. Mound, J. E. & Davies, C. J. Longitudinal structure of Earth's magnetic field controlled by lower mantle heat flow. *Nat. Geosci.* **16**, 380–385 (2023).
59. Gubbins, D. Thermal core-mantle interactions: theory and observations. In Dehant, V., Creager, K., Karato, S., & Zatman, S. *Earth's*

Core: dynamics, structure and rotation (AGU Geodynamics Series - American Geophysical Union, 2003).
60. Aubert, J., Amit, H., Hulot, G. & Olson, P. Thermo-chemical wind flows couple Earth's inner core growth to mantle heterogeneity. *Nature* **454**, 758–761 (2008).
61. Tauxe, L. et al. PmagPy: Software package for paleomagnetic data analysis and a bridge to the Magnetics Information Consortium (MagIC) Database. *Geochem. Geophys. Geosyst.* **17**, 2450–2463 (2016).
62. Kirschvink, J. L. The least-squares line and plane and the analysis of palaeomagnetic data. *Geophys. J. Int.* **62**, 699–718 (1980).
63. Tauxe, L. & Staudigel, H. Strength of the geomagnetic field in the Cretaceous Normal Superchron: New data from submarine basaltic glass of the Troodos Ophiolite. *Geochem. Geophys. Geosyst.* **5**, 1–16 (2004).
64. Aster, R. C., Borchers, B. & Thurber, C. H. *Parameter estimation and inverse problems* (Elsevier, 2012).
65. Cox, A. The frequency of geomagnetic reversals and the symmetry of the nondipole field. *Rev. Geophys.* **13**, 35–51 (1975).
66. McElhinny, M. W., McFadden, P. L. & Merrill, R. T. The time-averaged paleomagnetic field 0-5 Ma. *J. Geophys. Res. Solid Earth* **101**, 25007–25027 (1996).
67. Terra-Nova, F. & Wardinski, I. Regional outer core kinematics from the time dependence of intense geomagnetic flux patches. *Phys. Earth Planet. Inter.* **344**, 107106 (2023).
68. Olson, P. & Amit, H. Changes in Earth's dipole. *Naturwissenschaften* **93**, 519–542 (2006).
69. Gubbins, D. & Roberts, N. Use of the frozen-flux approximation in the interpretation of archaeomagnetic and paleomagnetic data. *Geophys. J. R. Astr. Soc.* **73**, 675–687 (1983).
70. Johnson, C. L. & Constable, C. G. The time-averaged geomagnetic field: global and regional biases for 0-5 Ma. *Geophys. J. Int.* **131**, 643–666 (1997).

Acknowledgements

The authors appreciate Richard Holme and anonymous reviewers for their suggestions and useful comments, and the editorial work of Laura Frahm. Authors thank the grants #2022/03086-2, #2023/04179-7, #2023/13612-6, São Paulo Research Foundation (FAPESP). G.A.H. and W.P.O thank to National Council for Scientific and Technological Development (CNPq) (#312737/2020-3, #150796/2022-6, #305110/2023-3). J.F.S. also thanks CNPq for grants #304022/2018-7 and #311231/2021-7. F.T.-N. was supported by the Centre national d'études spatiales (CNES). This work was conducted at the Paleomagnetism Laboratory USPMag, at the Instituto de Astronomia, Geofísica e Ciências Atmosféricas (IAG), Universidade de São Paulo (USP) and is financially supported by FAPESP/CAPES/CNPq.

Author contributions

W.P.O, G.A.H and F.T.N contributed to design of this study, performed the analyses and write the original draft. W.P.O and F.T.N designed the geomagnetic field models presented in the article. N.G.P, J.F.S, E.F.L and F.R.L contributed to the data collection. All the above authors and R.I.F.T. contributed to the final version of the manuscript.

Competing interests

The authors declare no competing interests.

Additional information

Supplementary information The online version contains supplementary material available at https://doi.org/10.1038/s41467-024-53688-2.

Correspondence and requests for materials should be addressed to Wellington P. de Oliveira.

Peer review information *Nature Communications* thanks the anonymous reviewers for their contribution to the peer review of this work. A peer review file is available.